Magn Reson Med Sci 2021; 20; 28–33
doi:10.2463/mrms.mp.2019-0201
Published Online: March 6, 2020

MAJOR PAPER

Peritumoral Fat Content Correlates with Histological Prognostic Factors in Breast Carcinoma: A Study Using Iterative Decomposition of Water and Fat with Echo Asymmetry and Least-squares Estimation (IDEAL)

Sachi Hisanaga[1], Takatoshi Aoki[1*], Shohei Shimajiri[2], Akitaka Fujisaki[1], Toshiyuki Nakayama[2], Masanori Hisaoka[3], Yoshiko Hayashida[1], Yuzuru Inoue[4], Yuko Tashima[5], and Yukunori Korogi[1]

Purpose: To correlate peritumoral fat content using iterative decomposition of water and fat with echo asymmetry and least-squares estimation (IDEAL) with histologic prognostic factors in breast carcinoma.

Methods: This study consisted of 100 patients who were diagnosed with invasive carcinoma of breast and underwent breast MRI including IDEAL before surgery. The scan time of IDEAL fat fraction (FF) map imaging was 33 s. Four regions of interests (ROIs), which are a distance of 5 mm from the tumor edge, and one ROI in the mammary fat of the healthy side were set on the FF map. Then average peritumoral FF values (FFt), average FF values in the healthy side (FFh), and peritumoral fat ratio (pTFR: defined as FFt/FFh) were calculated. Histologically, the presence of lymph node metastasis and the MIB-1 index were evaluated.

Results: FFt and pTFR for breast carcinoma with lymph node metastasis (79.27 ± 10.36 and 0.897 ± 0.078) were significantly lower than those without (86.23 ± 4.53 and 0.945 ± 0.032) ($P < 0.001$ and $P = 0.005$). Spearman rank correlation suggested that the FFt correlated with the MIB-1 index ($r = -340$, $P = 0.001$).

Conclusion: Quantification of peritumoral fat using IDEAL-iron quantification is associated with the histologic prognostic factors, and may be a practical tool for therapeutic strategy of breast carcinoma.

Keywords: *breast carcinoma, peritumoral fat, iterative decomposition of water and fat with echo asymmetry and least-squares estimation, magnetic resonance imaging, histologic prognostic factors*

Introduction

Invasive cancer cells have a dramatic impact on surrounding adipocytes in breast tissue.[1] Adipocytes in the vicinity of the cancer cells display profound phenotypic and functional alterations. These adipocytes are called cancer-associated adipocytes (CAAs). Their ability to secrete soluble factors such as IL-6, hepatocyte growth factor (HGF), exosomes and extra-cellular matrix components such as MMP-11 and collagen IV, which stimulate invasive properties of tumor cells.[2] Both *in vitro* and *in vivo*, CAAs located around breast cancer exhibit a decrease in lipid content, a decreased expression of adipocyte markers, and an activated state indicated predominantly by the overexpression of proinflammatory cytokines.[3] Histologically, CAAs located around breast cancer also consistently showed a decrease in both cell number and cell size compared with adipocytes distant from the tumor.[4] In addition, the release of the peritumoral cytokines and extracellular matrix leads to edema due to vascular permeability and fibroblast proliferation.[5] These histological changes can result in a decrease of the peritumoral fat proportion in breast tissue.

Currently available MRI has been used for determination of fat content in multiple organs. Iterative decomposition of water and fat with echo asymmetry and least-squares

[1]Department of Radiology, University of Occupational and Environmental Health School of Medicine, Fukuoka, Japan
[2]Department of Pathology and Cell Biology, University of Occupational and Environmental Health, Fukuoka, Japan
[3]Department of Pathology and Oncology, University of Occupational and Environmental Health, Fukuoka, Japan
[4]First Department of Surgery, University of Occupational and Environmental Health, Fukuoka, Japan
[5]Second Department of Surgery, University of Occupational and Environmental Health, Fukuoka, Japan

[*]Corresponding author: Department of Radiology, University of Occupational and Environmental Health, 1-1 Iseigaoka, Yahatanishi-ku, Kitakyushu, Fukuoka 807-8555, Japan. Phone: +81-93-691-7264, Fax: +81-93-692-0249, E-mail: a-taka@med.uoeh-u.ac.jp

Received: November 14, 2019 | Accepted: January 17, 2020

estimation (IDEAL) imaging is a promising fat quantitative method that can steadily separate fat and water by using the multi-point Dixon method and is implemented with a multi-echo three-dimensional spoiled gradient-echo acquisition.[6] Currently, IDEAL-iron quantification (IDEAL-IQ) method is increasingly used in the research field of lipid metabolism.[7,8] However, to the best of our knowledge, no reports have documented the relationship between the peritumoral fat proportion obtained by IDEAL-IQ and biologic behavior of breast carcinoma in human. The purpose of this study was to correlate the peritumoral fat content obtained by IDEAL-IQ with established histologic prognostic factors in breast carcinoma.

Materials and Methods

Our Institutional Review Board approved this study and informed consent was waived.

Patients

We retrospectively evaluated 163 consecutive patients who were diagnosed with breast carcinoma and underwent breast MRI before surgical resection or biopsy at our institution from January 2014 to December 2016. Sixty-three patients were excluded from the analysis for the following reasons: 32 did not undergo breast MRI without IDEAL fat fraction (FF) map imaging, nine received neoadjuvant chemotherapy before MRI, 10 had low amount of breast fat not enough to measure peritumoral fat, 12 had diffusely spreading non-masslike/small tumors. The remaining 100 patients with 100 lesions (age range 36–83 years, median 62.7 years) were consecutively recruited in this study. Tumor sizes ranged from 5 to 56 mm (mean 20.2 mm). The immunohistopathological characteristics of the tumors are summarized in Table 1.

Table 1 Immunohistological characteristics of the 100 breast carcinomas

Estrogen receptor (ER)	Positive	73
	Negative	27
Progesterone receptor (PgR)	Positive	49
	Negative	51
Human epidermal growth factor receptor type2 (HER2)	Positive	36
	Negative	64
MIB-1	≥20	37
	<20	63
Tumor subtype	Triple negative – a spectrum of ER+/HER2-negative	15
	Hormone receptor-negative and HER2-positive	12
	Hormone receptor-positive and HER2-positive	24
	Hormone receptor-positive and HER2-negative	49
	High receptor, low proliferation, low grade (luminal A-like)	44
	Low receptor, high proliferation, high grade (luminal B-like)	5

MRI protocol

MRI was performed with a 3T MR imaging unit (Discovery MR750W 3T scanner, GE Healthcare, Waukesha, WI, USA) and an eight-channel breast coil. The patients underwent imaging in a prone position. All patients underwent MRI covering the bilateral breast, including axial and sagittal T_2-weighted imaging, axial diffusion-weighted imaging (b = 0, 1500), axial gadolinium-enhanced dynamic imaging and axial IDEAL-IQ. The IDEAL-IQ acquisition was performed before contrast enhanced imaging. For IDEAL-IQ, the following pulse sequences were used: six echoes/TR, TR: 6.9 ms, TE min: 0.9 ms, TE spacing: 0.9 ms, TE range: 0.9–5.4 ms, slice thickness: 8 mm, FOV: 44 × 44 cm, matrix: 256 × 256, scan time: 33 s.

Quantitative image assessment

Four 0.5-cm^2 region of interests (ROIs) on the FF map obtained by IDEAL-IQ were set. The selection of ROI was performed manually by one general radiologist. The calculator set four ROIs adjacent to the peritumoral fat on each crosshair radial, which were a distance of 5 mm from the tumor edge (Fig. 1).[9] Placement of ROIs within breast tissue and fibroglandular tissue was avoided, and the ROIs were set on the largest lesion when there were multifocal lesions. Post-contrast and diffusion-weighted images were used as references. Another ROIs in the mammary fat of the healthy side were set on the FF map. Then average peritumoral FF values (FFt), average FF values in the healthy side (FFh), and peritumoral fat ratio (pTFR: defined as FFt/FFh) were calculated.

Histopathological analysis

All of the histopathological specimens were reviewed for this study by two certificated pathologists who were blinded to the MRI findings and the final decision was reached by consensus. The MIB-1 index was determined by using the previously described semiquantitative visual method.[6] A quantitative assessment was made at 20 and/or 40 magnification by counting a total of 200–500 tumor cells within representative fields. All nuclei with homogeneous granular staining, multiple speckled staining or nucleolar staining were counted as positive, regardless of staining intensity. Cells with cytoplasmic staining were excluded. The histopathological characteristics in the vicinity of the breast carcinomas (5 mm apart from the tumor edge) were compared between breast carcinomas with lymph node metastasis and those without.

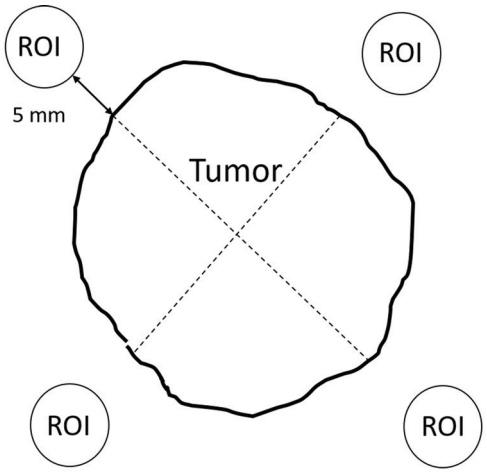

Fig. 1 Scheme illustrates peritumoral regions of interest (ROIs). Four ROI measuring 0.5-cm^2 on each crosshair radial were set.

Statistical analysis

The non-parametric Mann–Whitney *U* test was used to compare the FFt and the pTFR using IDEAL-IQ between breast carcinoma with lymph node metastasis and that without. Spearman rank correlation analysis was used to correlate the MIB-1 index with the FFt or the pTFR using IDEAL-IQ of breast carcinoma. The correlation between the tumor size and the FFt or the pTFR was also evaluated by Spearman rank correlation. A forward stepwise logistic regression model was used to identify variables that predicted lymph node metastasis, and the diagnostic performance of the best model was evaluated by receiver operating characteristic (ROC) analysis. A logistic model was used with age, tumor size, FFt, and pTFR. All calculations were performed by using IBM SPSS Statistics, version 22.0 (IBM, Armonk, NY, USA). The *P*-values <0.05 were considered statistically significant.

Results

The average FFt for breast carcinoma with lymph node metastasis (79.27 ± 10.36) was significantly lower than that without (86.23 ± 4.53) ($P < 0.001$) (Fig. 2). The pTFR for breast carcinoma with lymph node metastasis (0.897 ± 0.078) was also significantly lower than that without (0.945 ± 0.032) ($P = 0.005$) (Fig. 3). Spearman rank correlation suggested that the FFt and the pTFR correlated with the MIB-1 index ($r = -0.340$, $P = 0.001$; $r = -0.217$, $P = 0.03$) (Figs. 4 and 5). Correlation between the FFt and the tumor size was also identified ($r = -0.312$, $P = 0.002$). Result of stepwise logistic regression analysis indicated that tumor size and FFt were predictors of lymph node metastasis ($P < 0.001$). The area under the ROC curve of the best model included tumor size and FFt was 0.813 (95% CI: 0.718–0.907).

Figures 6 and 7 show representative cases of breast carcinoma with axillary lymph node metastasis and the high percentage of MIB-1 index (Fig. 6) and of breast carcinoma

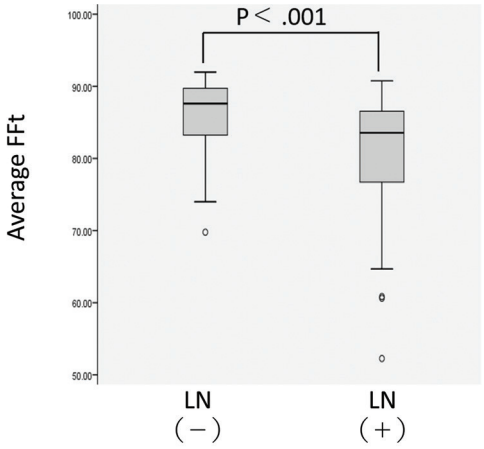

Fig. 2 Comparison of the peritumoral fat fraction values (FFt) between breast carcinoma with lymph node metastasis and that without. The average FFt for breast carcinoma with lymph node metastasis were significantly lower than that without ($P < 0.001$).

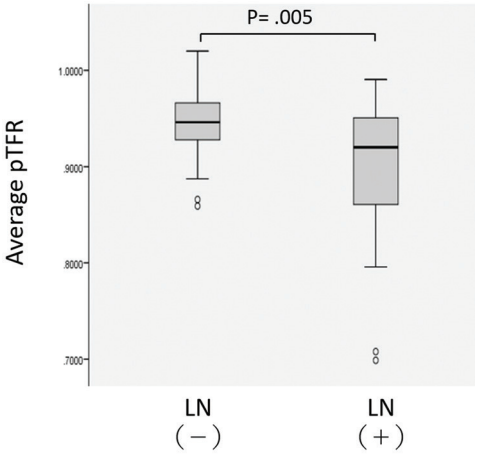

Fig. 3 Comparison of the peritumoral fat ratio (pTFR) between breast carcinoma with lymph node metastasis and that without. The pTFR for breast carcinoma with lymph node metastasis were also significantly lower than that without ($P = 0.005$).

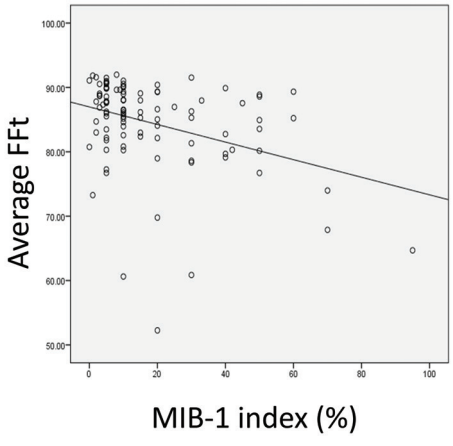

Fig. 4 Correlation between the MIB-1 index and the peritumoral fat fraction values (FFt). There is a significant negative correlation between the MIB-1 index and the FFt ($r = -0.340$, $P = 0.001$).

without axillary lymph node metastasis and the low percentage of MIB-1 index (Fig. 7). The average FFt value and the pTFR of the tumor on fat fraction map is low in breast carcinoma with axillary lymph node metastasis and the high percentage of MIB-1 index case. Whereas, in the breast carcinoma without axillary lymph node metastasis and the low percentage of MIB-1 index case, the average FFt value and the pTFR of the tumor on the fat fraction map is high.

Pathologically, peritumoral adipose tissue of breast carcinoma with lymph node metastasis revealed more fibrous and edematous compared with that without. In addition, atrophy of adipocyte and mild inflammatory cell infiltration tended to be more common in the peritumoral adipose tissue of breast carcinoma with lymph node metastasis (Fig. 8).

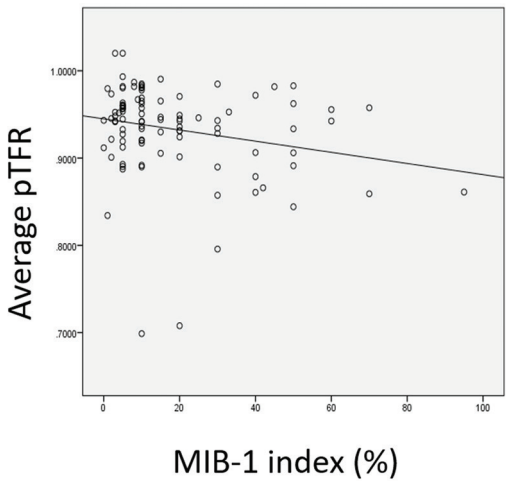

Fig. 5 Correlation between the MIB-1 index and the peritumoral fat ratio (pTFR). There is a significant negative correlation between the MIB-1 index and the pTFR ($r = -0.217$, $P = 0.03$).

Discussion

Cell proliferation is a major determinant of the biologic behavior of breast carcinoma, and MIB-1 monoclonal antibody is a promising tool for determining cell proliferation on routine histological material.[10] It is also known that axillary lymph node status is one of the most important prognostic variables for the management of patients with primary breast cancer.[11,12] Our study showed the peritumoral fat proportion using IDEAL-IQ was correlated with these established histologic prognostic factors. Quantification of the peritumoral fat content using IDEAL-IQ may predict the histologic prognostic factors *in vivo*.

Cancer cells secrete soluble factors leading to adipocyte "dedifferentiation". Adipocytes undergo morphologic changes, first marked by a decrease in adipocyte size and lipid content, then by acquiring a fibroblast-like morphology, yet still containing small lipid droplets.[13] Namely, mature adipocytes located around breast cancer lose their lipid content upon exposure to tumor cells and exhibit fibroblast-like morphology highlighting that they contribute to the cancer-associated fibroblast population. In the pathological examination of this study, peritumoral adipose tissue of the breast carcinoma with lymph node metastasis revealed more fibrous,

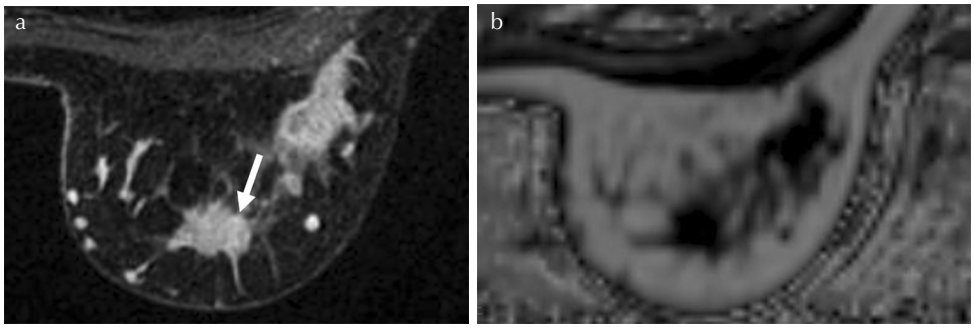

Fig. 6 Representative case of breast carcinoma with axillary lymph node metastasis and the high percentage of MIB-1 index. Fat-suppressed post-contrast T_1-weighted image (**a**) shows the enhancing mass (arrow) in the left breast, and the corresponding average peritumoral fat fraction values (FFt) (76.7) on the fat fraction map (**b**) and the peritumoral fat ratio (pTFR) (0.84) are low.

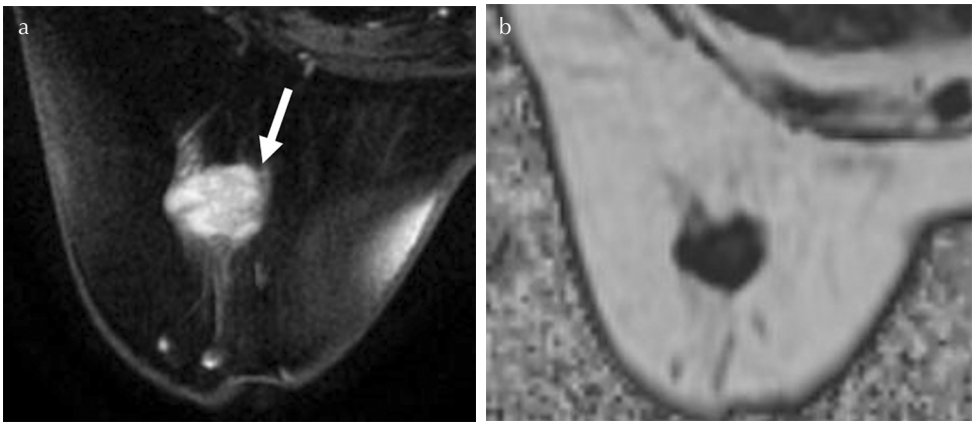

Fig. 7 Representative case of breast carcinoma without axillary lymph node metastasis and the low percentage of MIB-1 index. Fat-suppressed post-contrast T_1-weighted image (**a**) shows the enhancing mass (arrow) in the left breast, and the corresponding average peritumoral fat fraction values (FFt) (90.1) on the fat fraction map (**b**) and the peritumoral fat ratio (pTFR) (0.97) are high.

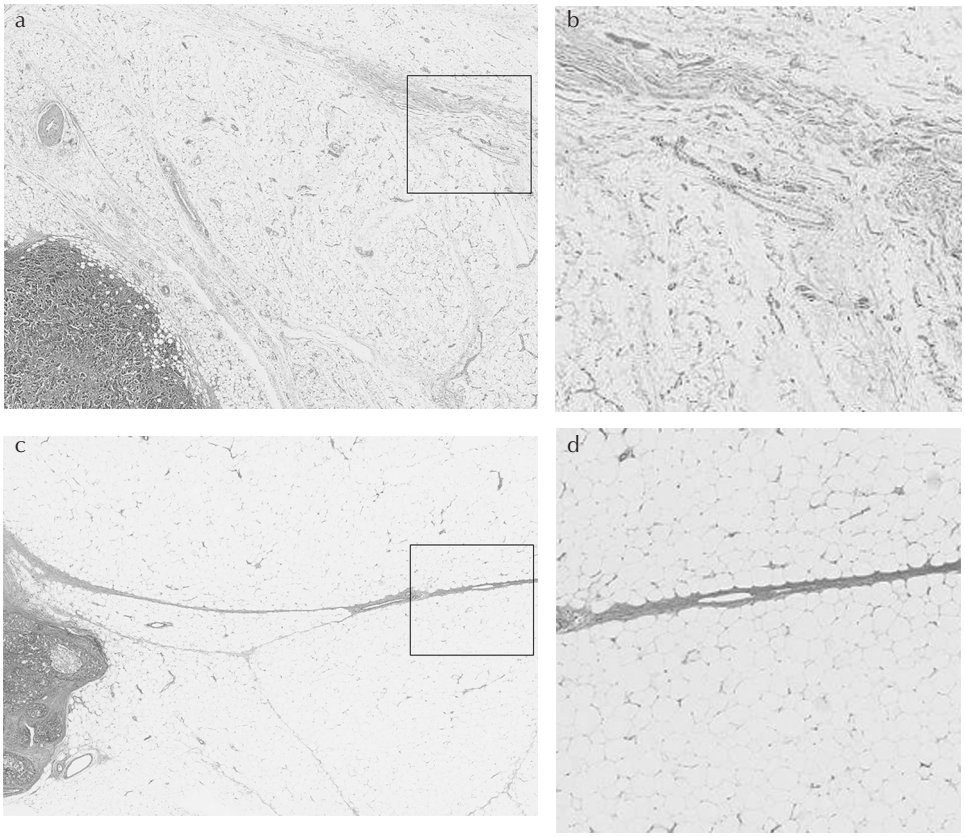

Fig. 8 Representative microscopic images of the peritumoral area of the breast carcinoma with axillary lymph node metastasis (**a**; low-power view of hematoxylin–eosin stain, **b**; magnified view of the square area of **a**) and that without (**c**; low-power view of hematoxylin–eosin stain, **d**; magnified view of the square area of **c**). Peritumoral adipose tissue of breast carcinoma with lymph node metastasis shows more fibrous and edematous (**a** and **b**) compared with that without (**c** and **d**). Atrophy of adipocyte and mild inflammatory cell infiltration are also seen in the peritumoral adipose tissue of breast carcinoma with lymph node metastasis (**a** and **b**).

edematous, and inflammatory compared with that without. This may be related to the CAA's ability to secrete soluble factors (IL-6, HGF, etc.) and exosomes and extra-cellular matrix components (MMP-11, collagen IV, etc.).[14–17] Peritumoral edema caused by the release of cytokines can also conduce to decrease the peritumoral fat proportion. Loss of the peritumoral fat content on IDEAL-IQ may reflect these pathological changes in the microenvironment of the breast.

Chemical shift-based water–fat separation techniques use an uncomplicated signal model that adopts a single resonant frequency for both water and fat. Nevertheless, T_2^* decay is a confounding factor to estimate fat content correctly in areas of irregular shape and abrupt changes between soft tissue and air, such as breast. Although MR spectroscopy is thought to be the most accurate method in quantifying fat–water content, an improvement in scan time and resolution is offered as practical quantitative imaging. Regarding fat fraction measurement, excellent correlation between T_2^*-corrected IDEAL method (known as IDEAL-IQ) and MR spectroscopy has been reported.[18] Recently, Yu et al.[19] demonstrated IDEAL-IQ achieved better water–fat separation and T_2^* estimation in breast compared with the previous method. Additionally, *in vivo* IDEAL-IQ can be performed in a short time and does not require an extrinsic contrast agent, and therefore IDEAL-IQ imaging adding to the conventional MRI may not be a burden on the patient with breast carcinoma. Although this method cannot be used in cases where there is a low amount of breast fat around the tumor, fat content measurement using IDEAL-IQ may be a practical tool for therapeutic strategy of breast carcinoma and can play a role in further radiomics study.

Our study had several limitations. First, diffuse spreading non-masslike lesions and lesions surrounded by the mammary gland tissue all the periphery mostly were not included in this study. The relationship between peritumoral fat content and prognostic biomarkers in these type tumors requires further study dealing with MRI-based radiomics and deep learning. Second, we manually set the ROIs for fat quantification without a reproducibility assessment. An automated ROI selection method would overcome the problems related to subjective ROI placement and might have improved the reproducibility. Third, we did not measure fat content pathologically. Direct MRI to pathology comparison would help for understanding biological response of peritumoral fat in patients with invasive breast carcinoma. Fourth, peritumoral fat content may have been contaminated by post-biopsy effects such as edema, although we set four ROIs adjacent to the peritumoral fat on each crosshair radial to reduce the effect of the postprocedural changes. A comparative study between subjective visual assessment of peritumoral edema and peritumoral fat quantitative assessment may be warranted. Finally, this study is inherently limited by its

retrospective nature. Additional prospective study with a large number of cases may be necessary to support our conclusions because there are substantial overlaps in the FFt and pTFR between breast carcinoma with lymph node metastasis and that without, and the correlations between the MIB-1 index and the FFt/pTFR are weak.

Conclusion

Our study suggests that the peritumoral fat content using IDEAL-IQ appear to show an association with histologic prognostic factors *in vivo*, and the peritumoral fat quantification using IDEAL-IQ, in combination with tumor size, may be useful for therapeutic strategy of breast carcinoma.

Conflicts of Interest

All authors do not have any conflicts of interest regarding the present study.

References

1. Duong MN, Geneste A, Fallone F, Li X, Dumontet C, Muller C. The fat and the bad: mature adipocytes, key actors in tumor progression and resistance. Oncotarget 2017; 8: 57622–57641.
2. Dirat BA, Bochet L, Escourrou G, Valet P, Muller C. Unraveling the obesity and breast cancer links: a role for cancer-associated adipocytes? Endocr Dev 2010; 19:45–52.
3. Nieman KM, Kenny HA, Penicka CV, et al. Adipocytes promote ovarian cancer metastasis and provide energy for rapid tumor growth. Nat Med 2011; 17:1498–1503.
4. Dirat B, Bochet L, Dabek M, et al. Cancer-associated adipocytes exhibit an activated phenotype and contribute to breast cancer invasion. Cancer Res 2011; 71:2455–2465.
5. Cheon H, Kim HJ, Kim TH, et al. Invasive breast cancer: prognostic value of peritumoral edema identified at preoperative MR imaging. Radiology 2018; 287:68–75.
6. Reeder SB, Wen Z, Yu H, et al. Multicoil Dixon chemical species separation with an iterative least-squares estimation method. Magn Reson Med 2004; 51:35–45.
7. Ma J, Song Z, Yan F. Detection of hepatic and pancreatic fat infiltration in type II diabetes mellitus patients with IDEAL-Quant using 3.0T MR: comparison with single-voxel proton spectroscopy. Chin Med J 2014; 127:3548–3552.
8. Guo RM, Li QL, Luo ZX, et al. In vivo assessment of neurodegeneration in type C Niemann-Pick disease by IDEAL-IQ. Korean J Radiol 2018; 19:93–100.
9. Lu S, Ahn D, Johnson G, Cha S. Peritumoral diffusion tensor imaging of high-grade gliomas and metastatic brain tumors. AJNR Am J Neuroradiol 2003; 24:937–941.
10. Spyratos F, Ferrero-Poüs M, Trassard M, et al. Correlation between MIB-1 and other proliferation markers: clinical implications of the MIB-1 cutoff value. Cancer 2002; 94:2151–2159.
11. Jatoi I, Hilsenbeck SG, Clark GM, Osborne CK. Significance of axillary lymph node metastasis in primary breast cancer. J Clin Oncol 1999; 17:2334–2340.
12. El Hage Chehade H, Headon H, El Tokhy O, Heeney J, Kasem A, Mokbel K. Is sentinel lymph node biopsy a viable alternative to complete axillary dissection following neoadjuvant chemotherapy in women with node-positive breast cancer at diagnosis? An updated meta-analysis involving 3,398 patients. Am J Surg 2016; 212:969–981.
13. Bochet L, Lehuédé C, Dauvillier S, et al. Adipocyte-derived fibroblasts promote tumor progression and contribute to the desmoplastic reaction in breast cancer. Cancer Res 2013; 73:5657–5668.
14. Wei HJ, Zeng R, Lu JH, et al. Adipose-derived stem cells promote tumor initiation and accelerate tumor growth by interleukin-6 production. Oncotarget 2015; 6:7713–7726.
15. Ribeiro RJ, Monteiro CP, Cunha VF, et al. Tumor cell-educated periprostatic adipose tissue acquires an aggressive cancer-promoting secretory profile. Cell Physiol Biochem 2012; 29:233–240.
16. Motrescu ER, Blaise S, Etique N, et al. Matrix metalloproteinase-11/stromelysin-3 exhibits collagenolytic function against collagen VI under normal and malignant conditions. Oncogene 2008; 27:6347–6355.
17. Monvoisin A, Bisson C, Si-Tayeb K, Balabaud C, Desmoulière A, Rosenbaum J. Involvement of matrix metalloproteinase type-3 in hepatocyte growth factor-induced invasion of human hepatocellular carcinoma cells. Int J Cancer 2002; 97:157–162.
18. Meisamy S, Hines CD, Hamilton G, et al. Quantification of hepatic steatosis with T1-independent, T2-corrected MR imaging with spectral modeling of fat: blinded comparison with MR spectroscopy. Radiology 2011; 258:767–775.
19. Yu H, Shimakawa A, Mckenzie CA, Brodsky E, Brittain JH, Reeder SB. Multiecho water-fat separation and simultaneous R2* estimation with multifrequency fat spectrum modeling. Magn Reson Med 2008; 60:1122–1134.